

# Dual Band Rectenna for Electromagnetic Energy Harvesting at 2.4 GHz and 5 GHz Frequencies

Lalbabu Prashad<sup>1,2</sup>, Harish Chandra Mohanta<sup>1</sup>, and Ahmed Jamal Abdullah Al-Gburi<sup>3,\*</sup>

<sup>1</sup>Department of ECE, Centurion University of Technology and Management, Bhubaneswar 752050, India

<sup>2</sup>Department of ECE, Raghu Engineering College, Vishakhapatnam 531162, India

<sup>3</sup>Center for Telecommunication Research & Innovation (CeTRI), Faculty of Electronics and Computer Technology and Engineering Universiti Teknikal Malaysia Melaka (UTeM), Jalan Hang Tuah Jaya, Durian Tunggal 76100, Melaka, Malaysia

**ABSTRACT:** This work investigates low-power electromagnetic energy harvesting at 2.4 GHz and 5 GHz using an elementary rectangular patch rectenna along with a step-up DC-DC boost converter. The receiving antenna is optimized to  $50\,\Omega$  impedance by tuning parasitic ground plane stubs in the resonating frequencies. The return loss and gain of the proposed antenna are  $-30.19\,\mathrm{dB}$ ,  $-31.02\,\mathrm{dB}$  and 2.45 dBi, 4.84 dBi at 2.4 GHz and 5 GHz, respectively. A single-stage Greinacher voltage multiplier with a compact dual-band pi-model matching circuit is proposed as a rectifier. The rectenna is manufactured on an FR4 substrate, and the measured performance is in good agreement with the simulated results. The transformation efficiency of more than 40% is noticed in the wide input-power range from  $-12\,\mathrm{dBm}$  to  $5\,\mathrm{dBm}$ . The maximum efficiency of 50% and DC output voltage of  $1.57\,\mathrm{V}$  at  $0\,\mathrm{dBm}$  input power with  $5.1\,\mathrm{K}\Omega$  optimized load resistance is noticed when the RF source and rectenna are  $46\,\mathrm{cm}$  apart. The proposed rectenna with a DC-DC boost converter can drive the LED indicator and wall clock simultaneously. The prototype rectenna is suitable for energizing low-power sensor nodes in IOT and WSN applications.

### 1. INTRODUCTION

n smart networks, wireless communication technologies co-Loperate to gather and analyze data from various sources like sensors, devices, and citizen interactions to boost aspects of life. Most sensors and internet of things (IoT) devices that require low input power are energized by batteries. The use of batteries in hazardous environment imposes maintenance costs and limited life cycles which interrupts the operation of sensors in smart networks. Recent developments in wireless technologies make these smart networks self-sustainable and ecofriendly using energy harvesting (EH) methods [1]. There are numerous ambient energies like vibration, wind, geothermal, tides, electromagnetic, and light. Solar energy is unlimitedly available compared to electromagnetic (EM) energy but suffers from unreachability in some locations. The wide spread of EM energy in habitats and the increasing density of transmitting sources like cellular base stations, Bluetooth devices, Wi-Fi routers, WLAN, WBAN, etc., makes the radio frequency (RF) or EM energy ubiquitous and the best choice for EH.

Harvesting RF power requires a receiving antenna, impedance matching circuit (IMC), and rectifier circuit. The receiving antenna picks up the available ambient EM energy in the surroundings and transfers it to the rectifier using IMC to reduce the loss amid the antenna and rectifier. The rectifier uses a nonlinear Schottky diode to transform the received input AC power to a DC output power. The Schottky diodes are preferred because of their very high speed, very low voltage

drop, and high conversion efficiency capability compared to CMOS. So, Schottky diode-based rectifiers are superior to CMOS-based rectifiers at microwave frequencies [2]. The overall transformation efficiency of the rectenna depends on available RF energy density, matching network performance, and rectifying components. The whole act of the EH system is based on the power gathered by the receiving antenna at the front end, to the transfer efficiency of the rectifier network. So, the more the RF power is at the front end, the more the obtained output power is. The selection of the proper frequency band and gain of the receiving RF antenna increase the power collected by the rectenna system. Multiband antennas are preferred because of their capability to collect more RF power than single-band antennas.

The architecture of the rectifiers with IMC is divided into three categories based on receiving frequencies, single-band [3–7], multi-band [8–14], and broad-band [15–17]. At low input power, a single-band rectifier with IMC has more power transfer efficiency but collects limited output DC power. In counterpart, the broad-band rectifier collects energy from the entire resonating frequency spectrum by sacrificing the Q-factor of the IMC, which degrades the power transformation efficiency of the rectenna. A trade-off between maximum power transformation efficiency and the DC power output is obtained by harvesting selective power from certain bands using a multi-band rectifier.

Various multi-band rectenna constructions have been reported by past researchers operating at Wi-Fi, GSM, WLAN, and LTE frequencies due to the prevalence of wireless net-

<sup>\*</sup> Corresponding author: Ahmed Jamal Abdullah Al-Gburi (ahmedjamal@ieee.org, engahmed\_jamall@yahoo.com).



works. In [18], an aperture-coupled multilayer dual-band antenna with a huge gain is proposed to harvest RF energy at 3.5 GHz and 5.8 GHz using a dual-band rectifier that achieves 44% and 29% conversion efficiencies in the corresponding operating bands with an output voltage of 656.88 mV at 0 dBm input power. High gain is obtained by optimizing rectangular cells etched on a patch using a genetic algorithm. In [19], a harmonic suppression pi-shaped slot etched dual-band rectenna is proposed to engage at 2.45 GHz and 5 GHz. To obtain high transformation efficiencies of 68.83% and 49.90%, optimized load resistances of 700 ohms and 1.1 k ohms are used, and DC voltages of 0.167 V and 0.236 V are obtained at 0 dBm RF low power input. A tri-band rectangular patch with corrugated tapered side edges is integrated with a Dickson voltage multiplier for RF-EH in the bands 2.4-2.5 GHz, 5-5.1 GHz, and 4-4.15 GHz. The proposed rectenna obtained 298 mV output DC power in the resonating bands [20]. Improving rectenna design to increase efficiency and power conversion involves optimizing antenna geometries [21, 22], rectifier circuits [23], and matching networks [24-26] to maximize energy conversion. In [27], a dual-band rectenna is steered to engage at 3.5 GHz and 5.8 GHz frequencies, and a rectangular dielectric resonator along a slotted ground plane is used to obtain circular polarization in the resonating bands. A single diode HSMS2860 rectifier topology with a transmission line and rectangular stub matching network is used to obtain maximum power conversion efficiencies (PCEs) of 54.53% and 41.26% with 1.31 V and 1.16 V output voltages at respective operating frequencies observed for 5 dBm input power. In [28], a dual-band compact slot receiver is designed on an FR4 dielectric substrate to harvest electromagnetic energy at 5 GHz and 7.8 GHz frequencies. The RF harvester antenna has 4.7 dBi and 5.8 dBi realized gains in both operating bands. A Villard voltage doubler with SMS7630 and T-IMC is implemented for rectifying the received RF signal. The maximum PCE of 49.3% with 0.67 V is obtained at  $-10 \, dBm$  input power when both frequencies are applied simultaneously with a fixed load of  $1 \text{ K}\Omega$  throughout the measurement. In [29], a circular monopole coplanar waveguide (CPW) feed receiver with improved bandwidth from 0.9 to 3 GHz is acquired by etching 4 elliptical slots on the radiating patch and 4 slots symmetrically etched on the ground plane with a greater gain than 2.5 dBi in the entire bandwidth. A simple voltage rectifier is implemented using an SMS7630 diode with parallel and series inductors along the transmission line IMC to control the diode. The maximum PCEs of 45% and 33% with 366 mV and 170 mV are observed at 1.98 MHz and 1.88 MHz with  $-7 \, dBm$  and 3.56  $\mu W/cm^2$  when optimum loads of 1.5 K $\Omega$  and 0.9 K $\Omega$  are connected in the indoor calibration setup with 1 m separation between RF source and rectenna. A high-gain 2-layer disc radiator with a circular defected reflector arrangement is placed back at a length of  $\lambda/8$  to the disc patch. The maximum gains of 8.3 dBi and 7.8 dBi are obtained at 1.95 GHz and 2.45 GHz, respectively. The dual-band voltage doubler, consisting of an HSMS2850 diode and a 4-section IMC, is designed to achieve and measure maximum PCEs of 63% and 69% at both the operating frequencies with 1 K $\Omega$  load and 14 dBm and 15.5 dBm input power range. All the calibrations are observed when the RF source and rectenna are 40 cm

apart [30]. In [31], an omnidirectional dual-band rectenna operating at 2.45 GHz and 5.8 GHz is proposed with 65.1% and 38.4% PCEs and an optimum load of 1.2 K $\Omega$ . In the above-stated literature, either antenna design or IMC design is complex due to the stacking of multiband receivers which makes rectenna bulky. So single dual-band IMC with rectifier and single dual-band RF receiver are more suitable in IoT/WSN applications.

In this work, the electromagnetic energy harvesting at Wi-Fi frequencies 2.4 GHz and 5.0 GHz is proposed. For this purpose, a rectangular patch antenna along a parasitic ground stub is designed for RF energy harvesting at Wi-Fi frequencies, and an HSMS2852 Schottky diode Greinacher voltage multiplier topology with Pi-section IMC is proposed for RF AC-DC transformation. For the antenna  $S_{11}$  plot, parametric analysis of the parasitic ground and partial ground plane, radiation pattern, and current distribution have been presented, and power transfer efficiencies of the rectifier with and without Pi-section IMC have been simulated and compared with the measured results to authenticate the act of the rectenna.

# 2. PROPOSED RECTENNA CONSTRUCTION

# 2.1. Construction of the RF Receiving Antenna

A simple rectangular patch antenna with partial ground along parasitic stubs (PGPSs) in the ground plane is simulated and fabricated on dielectric FR4 material with  $\varepsilon_r=4.3$  and 0.025 loss tangent with the height of 1.6 mm and conductive copper thickness of 0.05 mm on both sides of the dielectric material. A 50  $\Omega$  microstrip feedline is used to drive the patch. The overall length  $(S_L)$  and width  $(S_W)$  of the antenna are  $60\times50\,\mathrm{mm}^2$ . The detailed geometry and fabricated prototype of the recommended antenna are depicted in Figure 1, whereas the geometrical dimensions of the prototype antenna are shown in Table 1.

**TABLE 1**. The rectangular patch with PGPS antenna optimized dimensions.

Variables	Value (mm)	Variables	Value (mm)	
$S_L$	60	$G_L$	14	
$S_W$	50	$G_W$	50	
$P_L$	23	$T_{L1}$	16.5	
$P_W$	30	$T_{W1}$	8	
$F_L$	15	$T_{L2}$	15	
$F_W$	2.8	$T_{W2}$	30	
G	1			

The dimensions of the rectangular patch antenna are calculated using basic design equations [32]. The prototype antenna evaluation steps are depicted in Figure 2. The recommended RF receiving antenna model starts with the first phase, a microstrip line feeding rectangular patch with the full ground (FG) plane. In the second phase, the FG plane is changed to a partial ground (PG) plane, and its height is optimized to obtain the impedance matching at the lower resonating frequency of 2.4 GHz. In the third phase, a rectangular parasitic stub T2 is placed above the

76



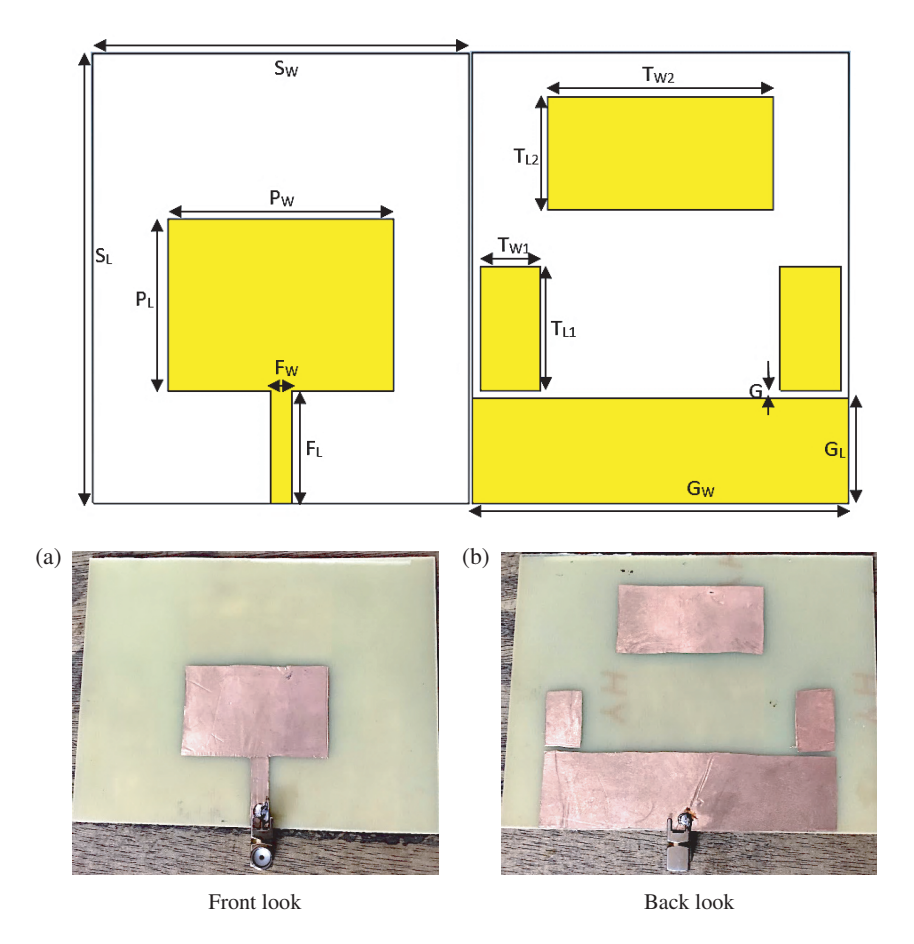


FIGURE 1. Detailed construction and manufactured pictures of the rectangular patch antenna with PGPS.

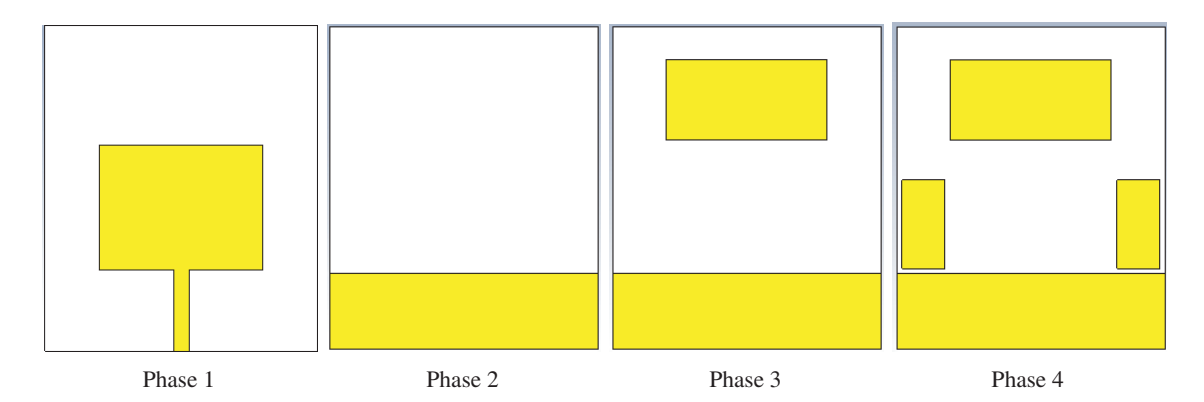
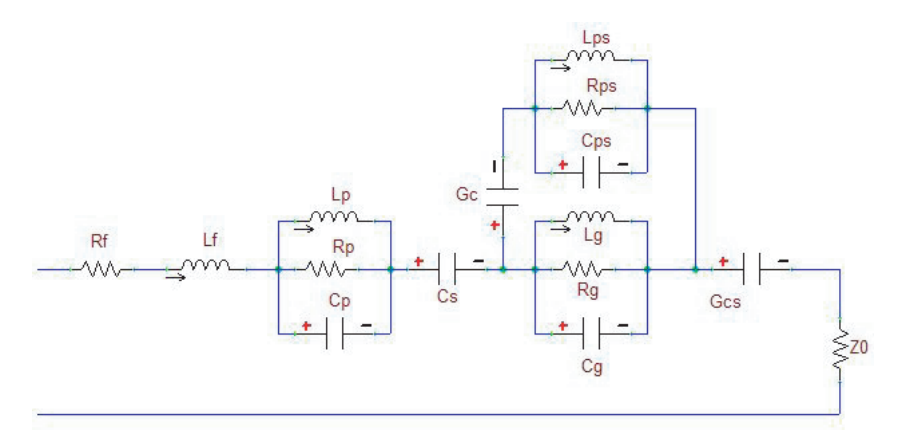


FIGURE 2. Evaluation steps of the simulated prototype receiving antenna.

radiating patch in the bottom plane to boost the bandwidth of the prototype antenna. Finally, in the fourth phase, two rectangular parasitic stubs T1 are placed on both sides of the radiating patch in the bottom plane to obtain the second resonating frequency of 5.0 GHz. All the dimensions in the four evaluation steps are optimized to obtain the 50  $\Omega$  impedance matching at both operating frequencies by using CST microwave studio.

A rectangular patch antenna can be realized with lumped elements as a parallel sequence of  $R_p, C_p$ , and  $L_p$ . The PG plane is realized as a parallel sequence of  $R_g, C_g$ , and  $L_g$ , and the parasitic rectangular stubs are also realized as a parallel sequence of

 $R_{ps}$ ,  $C_{ps}$ , and  $L_{ps}$ . At low frequencies, the rectangular equivalent circuits and PG plane are in resonance with mutual capacitance  $C_S$ . On the other hand, the partial ground plane along with the parasitic rectangular stub equivalent circuit is at resonance with mutual coupling capacitance  $G_C$  at a higher frequency, and both these resonating circuits are coupled through mutual capacitance  $G_{CS}$  at the output. The lumped model of the receiver is realized based on the current distribution. The equivalent lumped representation of the prototype receiver is depicted in Figure 3, and advanced design system (ADS) tool is used to simulate it. To validate the equivalent circuit of the



**FIGURE 3**. The proportionate lumped network of the prototype RF receiver.

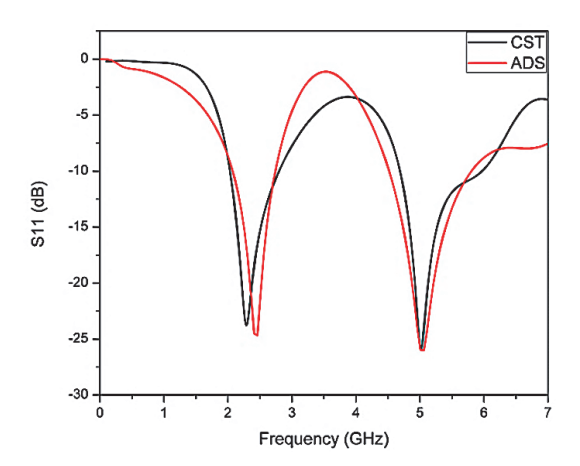


**FIGURE 4.** S-parameter correlation of the prototype receiver and its lumped network acquired from CST and ADS.

prospective receiver, it was modeled in ADS. The  $S_{11}$  of the CST-simulated antenna is correlated with the ADS equivalent circuit representation of the prototype receiver, and the comparison is displayed in Figure 4.

# 2.2. Design of the Rectifier with IMC

For electromagnetic/RF EH, the design of a rectifier model with a suitable diode presents a prominent role in the transformation of RF AC-DC power. The characteristics required in the diode for the rectifier must have low saturation current, forward voltage, junction capacitance, low input power level operating ability, and fast switching speed at high frequencies with optimum input impedance and have wide input power range operation capability necessary. Agilent Avago Technology provides HSMS-2852 Schottky diode which belongs to the HSMS-285x series and has a low saturation current  $I_S=3~\mu\text{A}$ , low forward voltage of 150 mV, low junction capacitance  $C_{J0}=0.18~\text{pF}$ , and a breakdown voltage of 3.8 V mostly matches the requirement for the prototype rectifier to work at wide-low input power level.

The ADS tool with a co-simulation harmonic balance (HB) controller was used to explore the parameters of the recommended rectifier with IMC. During the entire simulation pro-

cess of the rectifier, a  $50\,\Omega$  internal impedance power source is utilized instead of an RF receiver. The recommended rectifier with IMC is shown in Figure 5.

A one-stage Greinacher voltage doublet is used as a rectifier because of its simple design, cost-effectiveness, and compact solution for high voltage generation. The rectifier circuit is composed of an RF pass capacitor  $C_1=100\,\mathrm{pF}$ , a shunt capacitor (RF short)  $C_2=100\,\mathrm{pF}$ , and an HSMS-2852 Schottky diode (package consists of two diodes connected in series) for rectifying the incoming RF AC signal into usable output DC signal with an optimal load resistance of 5.1 K $\Omega$ . To gain the maximum power transmission amid the RF receiver and rectifier network, IMC is used to approximate the impedance of the receiver with rectifier impedance. In this work, IMC is realized as a pair of cascaded L-sections arranged in the Pi-section model. The L-section components of the IMC are calculated analytically by the following equations [33].

For high-frequency impedance matching, the component values are obtained by

$$\frac{1}{X_{CM}} = \frac{1}{Z_0} \sqrt{\frac{(Z_0 - R_L)}{R_L}} \tag{1}$$

$$X_{LM} = \sqrt{R_L (Z_0 - R_L)} - X_L$$
 (2)

where  $X_{CM}$  and  $X_{LM}$  are the impedance matching reactance of the capacitor and inductor, respectively;  $Z_0$  is the source impedance; and  $X_L$  and  $R_L$  are the imaginary and real parts of the rectifier impedance at high frequency.

For low-frequency impedance matching, the component values are obtained by

$$\frac{1}{X_{LM}} = \frac{1}{Z_0} \sqrt{\frac{(Z_0 - R_L)}{R_L}} \tag{3}$$

$$X_{CM} = \sqrt{R_L \left( Z_0 - R_L \right)} - X_L \tag{4}$$

www.jpier.org

where  $X_{LM}$  and  $X_{CM}$  are the impedance matching reactance of the inductor and capacitor, respectively;  $Z_0$  is the source impedance;  $X_L$  and  $R_L$  are the imaginary and real parts of the rectifier impedance at low frequency.

78



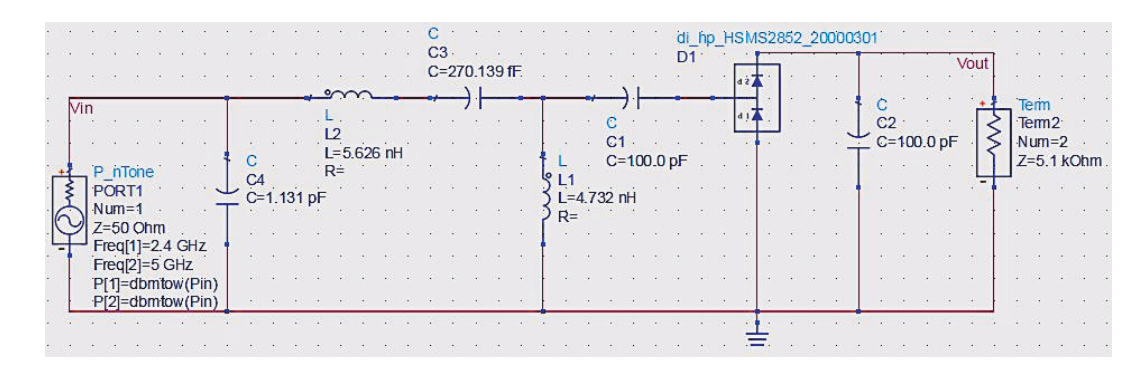


FIGURE 5. The simulated rectifier circuit with Pi-section IMC.

For impedance matching at a lower frequency of 2.4 GHz, an L-section IMC consisting of a series capacitor  $C_3=0.270\,\mathrm{pF}$  and parallel inductor  $L_1=4.7\,\mathrm{nH}$  is used to match the source impedance of  $50\,\Omega$  with  $9.81-j113.57\Omega$  rectifier impedance. The other L-section IMC at a higher frequency 5 GHz consists of a parallel capacitor  $C_4=1.13\,\mathrm{pF}$ , and series inductance  $L_2=5.63\,\mathrm{nH}$  is used to approximate the source impedance of  $50\,\Omega$  with  $7.61-j30.47\,\Omega$  rectifier impedance. The modified Pi-section IMC is optimized with the Smith chart matching utility tool in the ADS to obtain dual-band impedance matching at 2.4 GHz and 5 GHz. The theoretical and simulated lumped parameters of the modified Pi-section IMC are presented in Table 2.

**TABLE 2.** The theoretical and simulated lumped parameters of the modified Pi-section IMC.

Frequency (GHz)	Theoretical values	Simulated Values		
2.4	$C=0.397\mathrm{pF}$	$C=0.270\mathrm{pF}$		
2.4	$L=2.64\mathrm{nH}$	$L=4.73\mathrm{nH}$		
5	$C=1.5\mathrm{pF}$	$C=1.13\mathrm{pF}$		
3	$L=2.94\mathrm{nH}$	$L=5.63\mathrm{nH}$		

The RF power input is varied linearly from  $-30\,\mathrm{dBm}$  to  $20\,\mathrm{dBm}$ , and the RF AC-DC transfer efficiency for the dualtone ( $F_1=2.4\,\mathrm{GHz}$  and  $F_2=5\,\mathrm{GHz}$ ) power source is analyzed for optimum load resistance of  $5.1\,\mathrm{K}\Omega$  to plot the PTE and output DC-voltage of the rectifier with and without IMC. To understand the dual-band performance of the designed rectifier with modified Pi-section IMC, the prototype of the rectifier is manufactured on  $1.6\,\mathrm{mm}$  thick FR4 dielectric material, and the fabricated rectifier with IMC is shown in Figure 6.

#### 2.3. Step-up DC-DC Boost Converter Module

The output of the rectenna is high when it is connected to a load of a few tens of  $K\Omega$ , but in real-time applications, the sensors have a very low impedance which will degrade the efficiency of the rectenna. A voltage delivered by the rectenna must be stable to the functioning device voltage, and for this a step-up DC-DC boost converter is used to supply stable voltage to the sensors. An inductor-based step-up DC-DC boost converter with a low

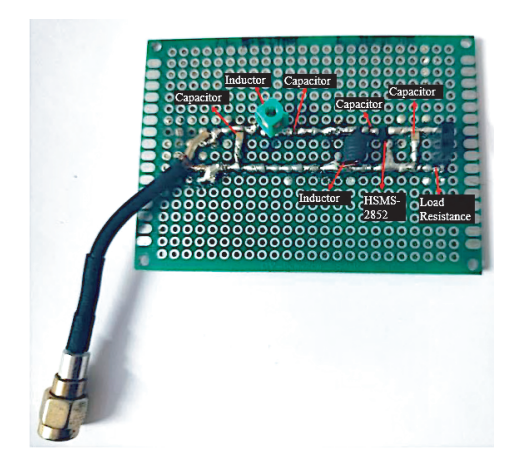


**FIGURE 6**. Pic of manufactured prototype rectifier with IMC.

start-up voltage of 0.8 V to generate a stable output voltage of 5 V is designed and fabricated to drive LED indicators.

The step-up DC-DC boost converter consists of an input capacitor  $C_1=100~\mu\mathrm{F}$ , inductor  $L_1=220~\mu\mathrm{H}$ , an SS14 Schottky diode, U1 2108A IC,  $C_2=C_3=10~\mu\mathrm{F}$ , and an output capacitance  $C_4=100~\mu\mathrm{F}$  is used. The circuit diagram, fabricated DC-DC boost converter, and functionality test of the boost converter are dispicted in Figure 7. In the fabricated boost converter, an LED indicator with a  $1~\mathrm{K}\Omega$  resistor is connected as load, and its functionality is verified by connecting to a regulated power supply (DC).

# 3. RESULTS AND DISCUSSION OF THE PROPOSED RECTENNA

# 3.1. Results and Discussion of the RF Receiving Antenna

The proposed RF receiving antenna performance analysis is carried out in the CST microwave studio. Figure 8 depicts the return loss plot of the phase-by-phase evaluation of the recommended receiver. In the first phase, the  $S_{11}$  plot shows that the receiver resonates at 5.9 GHz with a narrow bandwidth of 350 MHz (6.02–5.67 GHz) with -31 dB. By replacing the full ground (FG) plane with partial ground (PG) plane in the second step to improve the bandwidth, it is observed that the resonating frequency is changed from 5.9 GHz to 2.4 GHz, and also the bandwidth is increased to 1.63 GHz (3.08–2.17 GHz) with a re-



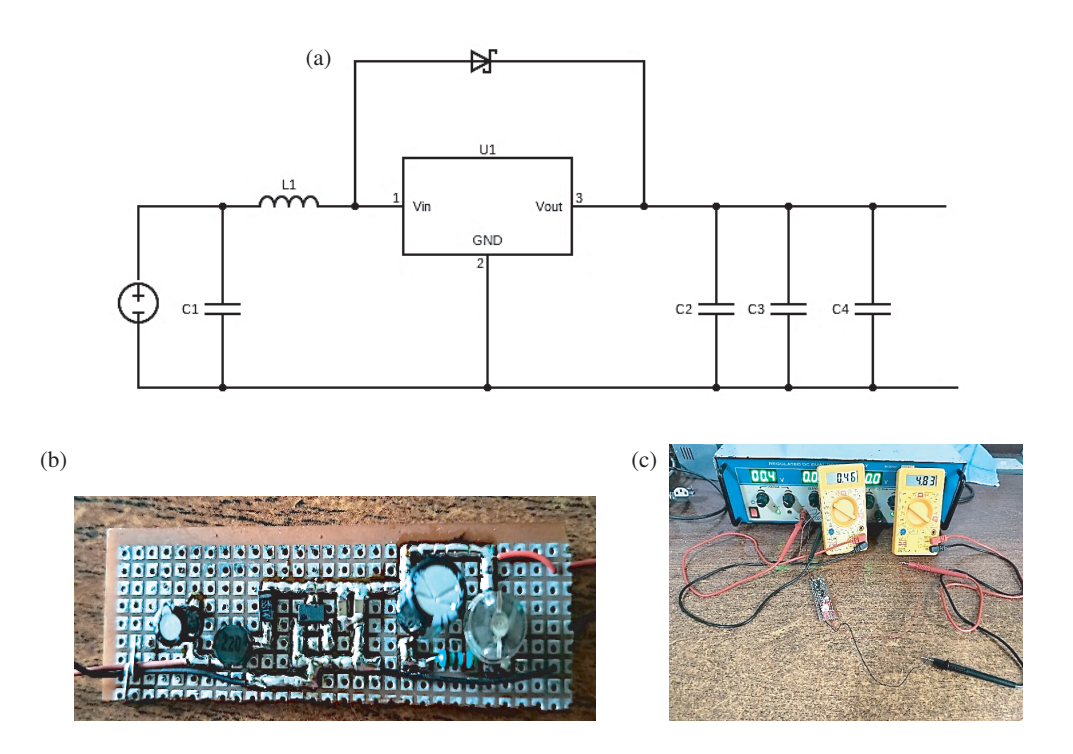
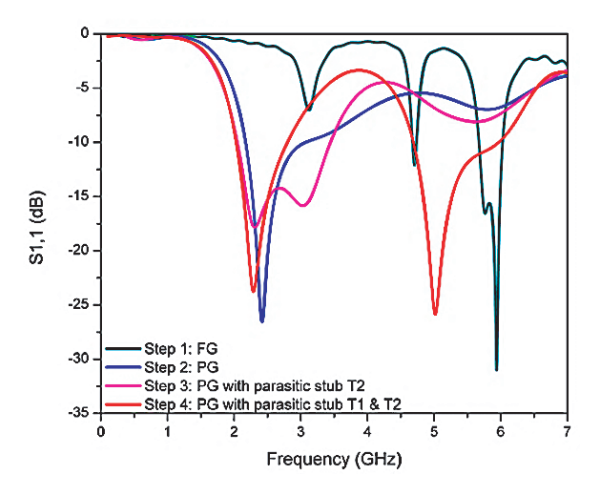
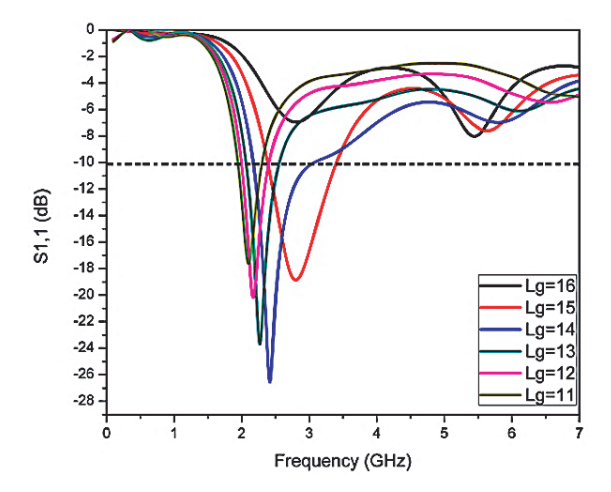


FIGURE 7. Step-up DC-DC boost converter, (a) circuit model, (b) fabricated pic, (c) Functionality test set-up.



**FIGURE 8**. Return loss plot of the simulated prototype antenna evaluation phases.



**FIGURE 9**. Return loss variations with parametric variations of PG plane length Lg.

turn loss of  $-26.54\,\mathrm{dB}$ . In the third step, by placing a rectangular parasitic stub2 in the bottom plane just above the patch, it is noticed that the  $S_{11}$  is reduced from  $-26.54\,\mathrm{dB}$  to  $-17.85\,\mathrm{dB}$ , but the bandwidth remains unchanged, and a small dip in the return loss at 5.3 GHz is obtained. In the fourth step, two resonating frequencies are observed at 2.32 GHz and 5 GHz with the  $S_{11}$  values of  $-23.7\,\mathrm{dB}$  with 760 MHz (2.04–2.8 GHz) bandwidth and  $-25.84\,\mathrm{dB}$  with 1.3 GHz (4.67–5.97 GHz) bandwidth, respectively by placing a pair of rectangular parasitic stub1 in the ground plane on either side of the patch.

The parametric approach has been conducted to understand the influence of discrete receiver variables on the impedance matching and operation of the receiver. At first, the length Lg of the PG plane is changed to investigate the antenna performance shown in Figure 9, by keeping the remaining parameters constant, and corresponding return loss values are plotted. It is observed that as the Lg decreased from 16 mm to 11 mm, the return loss values were much less than -10 dB and reached -25.8 dB at 2.4 GHz when Lg=14 mm and then increased slowly along with left shift in the resonating frequency as Lg further decreases. The proposed antenna resonates at the lower frequency of 2.4 GHz with a satisfactory  $|S_{11}|$  when the optimal PG plane length Lg is 14 mm.

Next, by changing the length  $(T_{L1})$  and width  $(T_{W1})$  of the parasitic stub1, its effect on the antenna performance is depicted in Figure 10. When the width  $T_{W1}$  is decreased from 10 mm



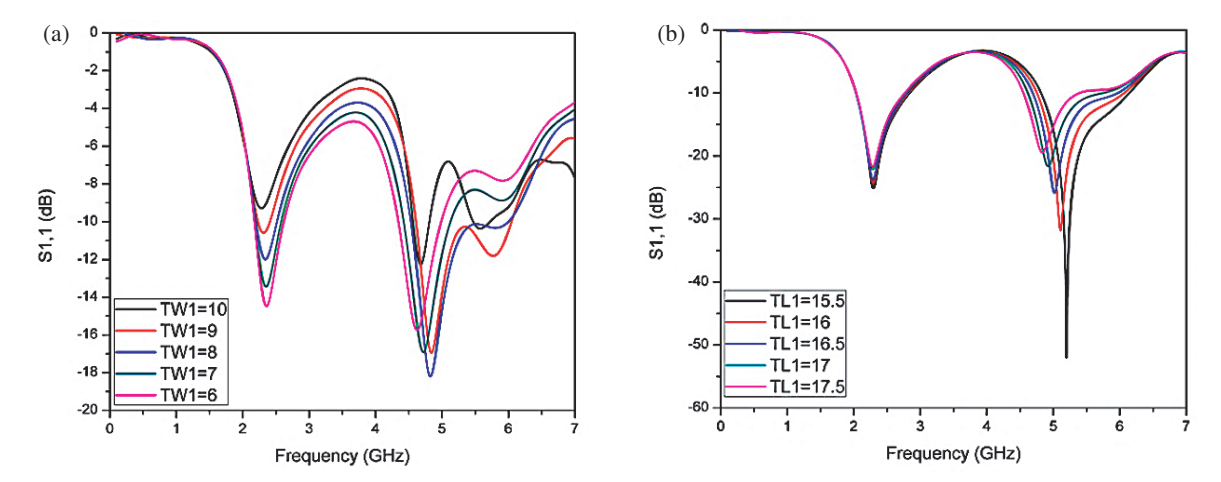


**FIGURE 10.** Return loss variations with parametric variations of parasitic stub1 (a) width  $T_{W1}$ , (b) length  $T_{L1}$ .

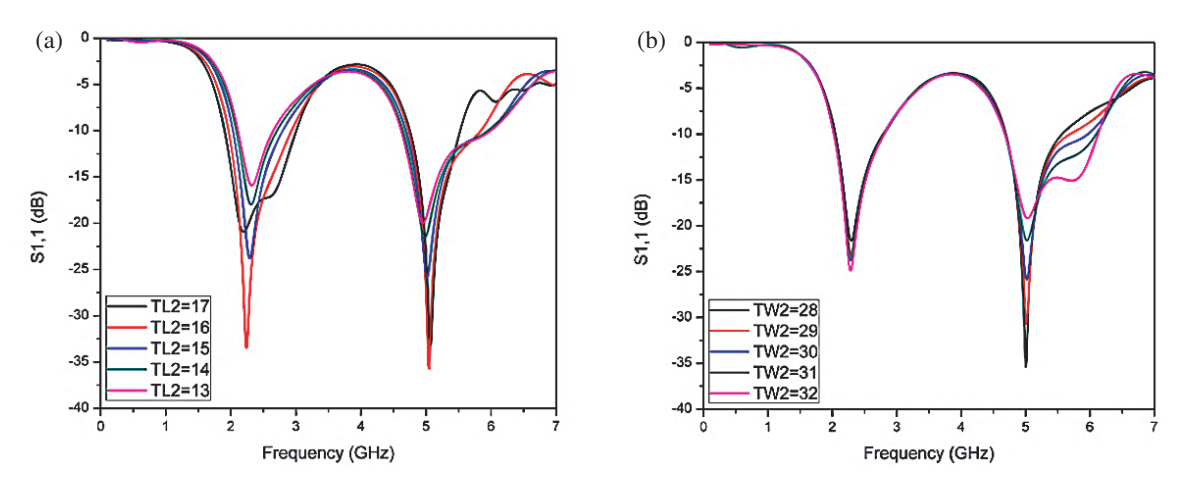


**FIGURE 11.** Return loss variations with parametric variations of parasitic stub2 (a) width  $T_{L2}$ , (b) length  $T_{W2}$ .

to 6 mm, dual-band characteristics are observed. As  $T_{W1}$  is decreased in step, the impedance matching improves amid the stub1 and radiating patch which results in the drop of return loss well below  $-10\,\mathrm{dB}$ , but as it is decreased further, the upper band and lower band move closer to one another. The optimum width of the parasitic stub  $T_{W1}=8\,\mathrm{mm}$  value is chosen because of the dual-band resonance at the desired Wi-Fi frequencies of 2.4 GHz and 5 GHz. When the length  $T_{L1}$  is increased from 15.5 mm to 17.5 mm, the lower band remains unchanged, but the upper band resonating frequency is fine-tuned both in impedance bandwidth and  $|S_{11}|$ . The optimum length  $T_{L1}=16.5\,\mathrm{mm}$  is chosen because proper impedance matching occurs amid the parasitic stub1 and the patch with return loss values  $-24.8\,\mathrm{dB}$  and  $-25.1\,\mathrm{dB}$  at  $2.37\,\mathrm{GHz}$  and  $5\,\mathrm{GHz}$ , respectively.

Finally, the effect of parametric variation in the parasitic stub2 on the performance of the receiver is shown in Figure 11. When the length  $T_{L2}$  of parasitic stub2 is varied, there is a considerable change in the resonating frequency with degradation in the return loss performance in both bands which are recorded as  $T_{L2}$  values are decreased from 17 mm to 13 mm. The optimum performance at both the resonant frequencies is observed when the  $T_{L2}$  value is set to 15 mm. When the width  $T_{W2}$  of

parasitic stub2 is increased from 28 mm to 32 mm, there is a reasonable effect in the resonating frequency with degradation in the return loss performance in the second resonating band. The required behavior of the receiver is recorded for both the resonating bands when  $T_{W2}$  is 30 mm.

The prototype receiver is intended for EM-EH in which receiving antenna impedance plays a fundamental role in modeling the IMC which acts as a bridge for energy transfer amid the receiver and rectifier. After parametric analysis, the optimum parameter values are chosen such that the proposed antenna impedance at both the resonating frequencies is close to  $50\,\Omega$ . The impedance real part and imaginary part of the antenna are  $50.0-j0.1\,\Omega$  and  $49.98-j0.6\,\Omega$  at 2.4 GHz and 5 GHz, respectively, which is shown in Figure 12(a). The simulated antenna radiation efficiency and gain versus frequency are displayed in Figure 12(b). At the resonating frequencies 2.4 GHz and 5 GHz, the radiation efficiency is 93% with a gain of 2.45 dBi and 79% with a gain of 4.84 dBi, respectively.

The current distribution on the surface of the prototype receiver at the resonating frequencies is shown in Figure 13. At 2.4 GHz and 5 GHz, the surface current of 64.7 A/m is observed. It is seen that more surface current is focused amid the parasitic stub1, PG plane, and radiating patch at the first



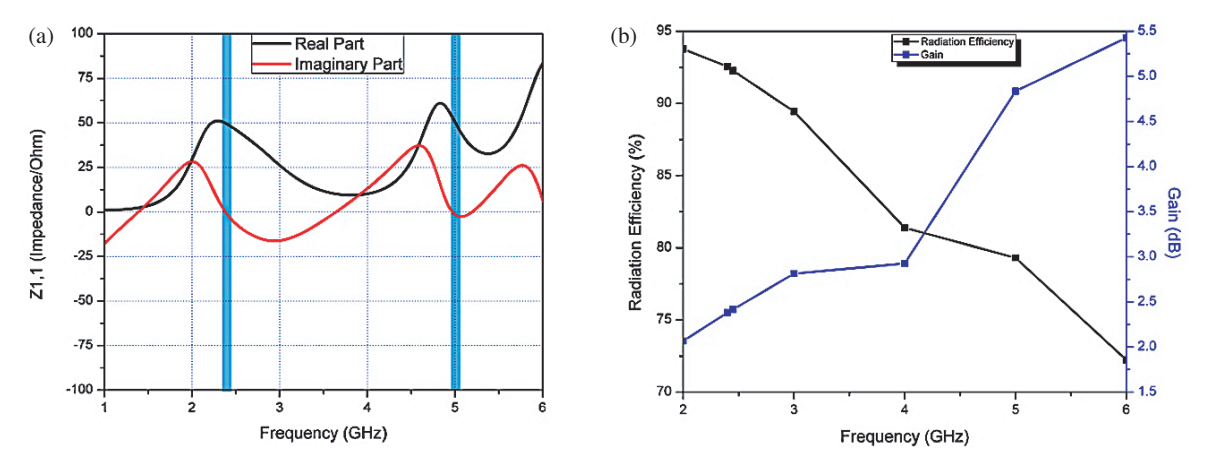


FIGURE 12. Recommended optimized receiver frequencies vs (a) impedance plot with real part and imaginary part. (b) Radiation efficiency and gain plot.

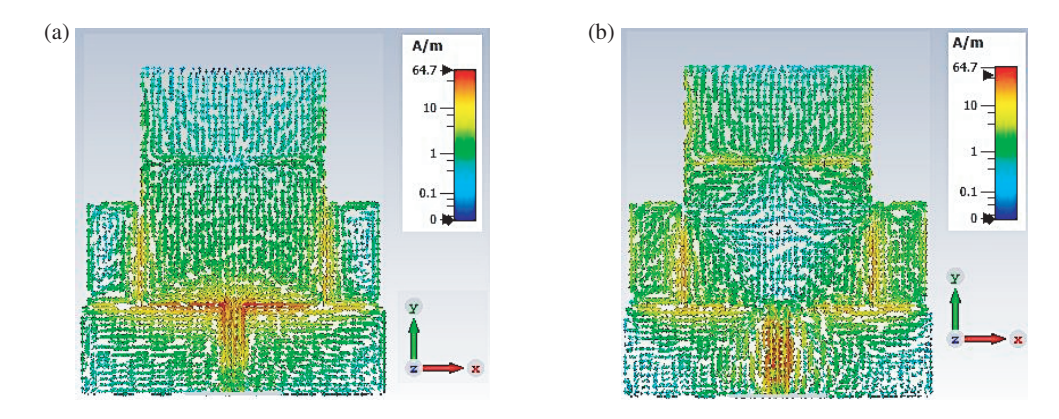


FIGURE 13. Prototype antenna surface current distribution at (a) 2.4 GHz and (b) 5.0 GHz.

resonating frequency, and for the second resonating frequency the maximum surface current is concentrated amid the parasitic stub1, stub2, PG plane, and radiating patch. Therefore, from the parametric analysis, the following is observed: as the width  $T_{W1}$  of parasitic stub1 varies, surface current distribution also changes which in turn changes the impedance matching and  $S_{11}$ of the receiver at both the working frequencies. When length  $T_{L1}$  is varied, the surface current will also change along the length but not width, so the corresponding effect on impedance bandwidth and return loss is seen in the second operating frequency but not in the first operating frequency. As surface current is distributed maximum on stub1 compared to stub2 for the 2.4 GHz when the width  $T_{W2}$  is changed, there is a negligible change in return loss at the lower band as more change is seen at the upper band. Similarly, as  $T_{L2}$  is varied the surface current concentration changes for both operating frequencies, so maximum variations are studied in return loss and impedance bandwidth at both bands.

The measured 2D polar plots of the receiver for the Eand H-plane radiation patterns in co-polar and cross-polar are
shown in Figure 14. At 2.4 GHz, the cross-polar is 40 dB less
than the co-polar magnitude in the E-plane, and in H-plane
the cross-polar is 82 dB less than the co-polar. It is noticed
that the omnidirectional radiation pattern is co-polar and bidi-

rectional in cross-polar. Similarly, at  $5\,\mathrm{GHz}$  the cross-polar is  $10\,\mathrm{dB}$  and  $83\,\mathrm{dB}$  less than the co-polar in E- and H-planes, respectively. An omnidirectional radiation pattern in co-polar and cross-polar is observed. From the radiation pattern characteristics, the prototype antenna radiates in all directions which is required for energy harvesting.

To validate the act of the receiving antenna in terms of  $S_{11}$ and impedance matching, it is measured by using Agilent technologies VNA E5071C ENA series. At first, the standard 1port short open load (SOL) is performed from 1 GHz to 7 GHz. The calibration setup and correlation of simulated and evaluated  $S_{11}$  outcomes of the prototype antenna are shown in Figure 15. From the measurement results it is recognized that the  $S_{11}$  value is improved at 2.4 GHz which reaches -30.19 dB and -31.02 dB at 5 GHz, but the impedance bandwidth is 405 MHz (2.39-2.8 GHz) at 2.4 GHz and 290 MHz (4.92-5.21 GHz) at 5 GHz in contrast with simulated results which is a little bit reduced. An additional band of 400 MHz (5.41-5.81 GHz) is observed in the calibration results with a center frequency of 5.62 GHz. The simulation and calibration results are in good correlation with each other. Moreover, the fabricated prototype antenna covers dual Wi-Fi bands of 2.4 GHz and 5 GHz. So the prototype of receiving antenna is suitable for Wi-Fi RF-EH.



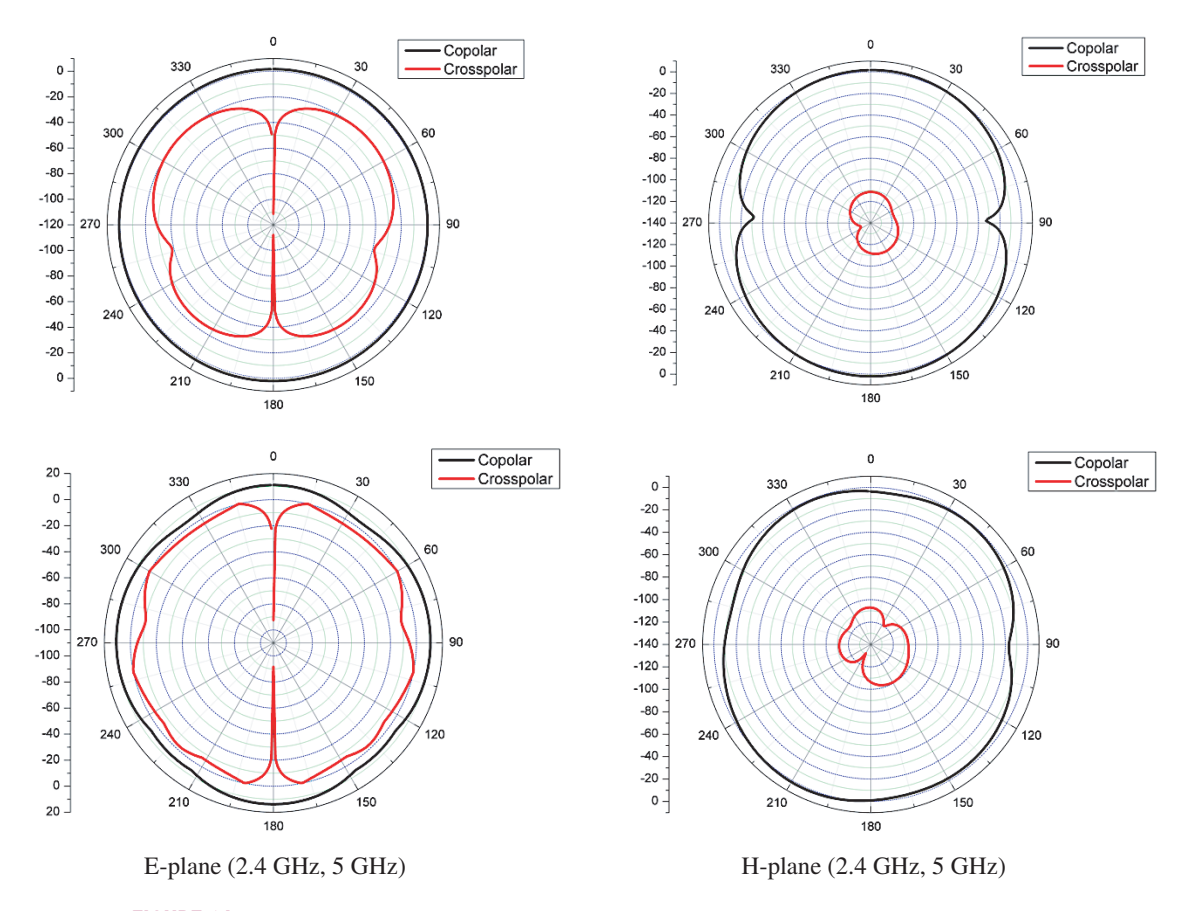


FIGURE 14. Measured polar plot of E- and H-plane of the receiver at 2.4 GHz and 5 GHz.

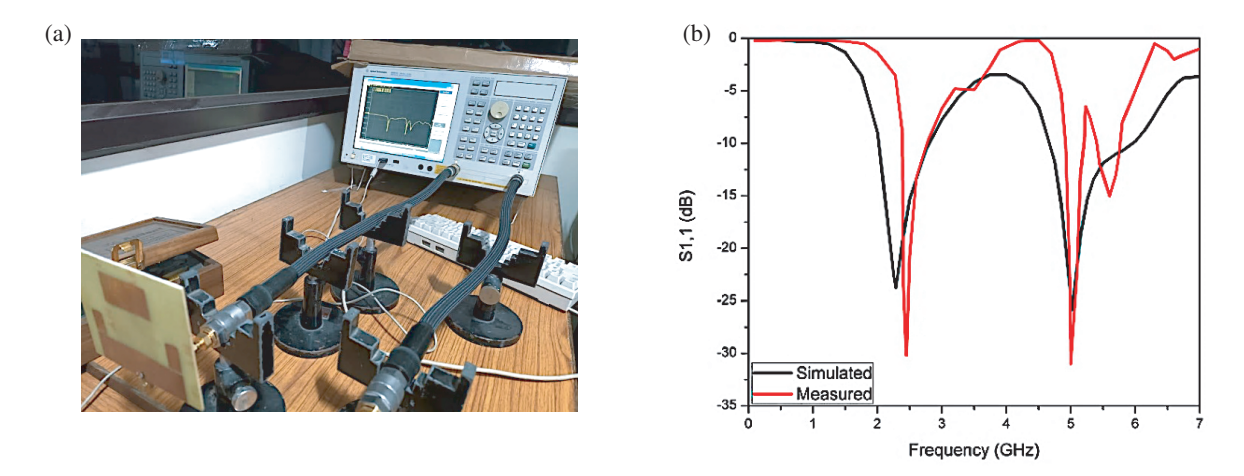


FIGURE 15. (a) Picture of the calibration system for the proposed RF receiving antenna. (b)  $S_{11}$  correlation plot of the calibration outcome with the simulated result for the manufactured prototype receiver.

# 3.2. Proposed Rectifier Network Results and Discussion

In the rectenna construction, rectifier performance is based on the RF AC-DC power transformation efficiency. In rectenna construction, the rectifier's performance is determined by the RF-to-DC power conversion efficiency, which measures how effectively the harvested RF AC power is transformed into usable DC power at the load. The power transformation efficiency (PTE) is the ratio of delivered load power to the rectifier power input, and it is acquired by Equation (5).

$$\eta_{AC\text{-}DC} = \frac{P_{deliverd\ DC}}{P_{input\ AC}} \times 100$$
 (5)

$$\eta_{AC\text{-}DC} = \frac{P_{deliverd\ DC}}{P_{input\ AC}} \times 100 \qquad (5)$$

$$P_{delivered\ DC} = \frac{\left(V_{delivered\ DC}\right)^2}{R_L} \qquad (6)$$

where  $P_{delivered\ DC}$  and  $V_{delivered\ DC}$  are the output DC power and voltage delivered to the load, respectively;



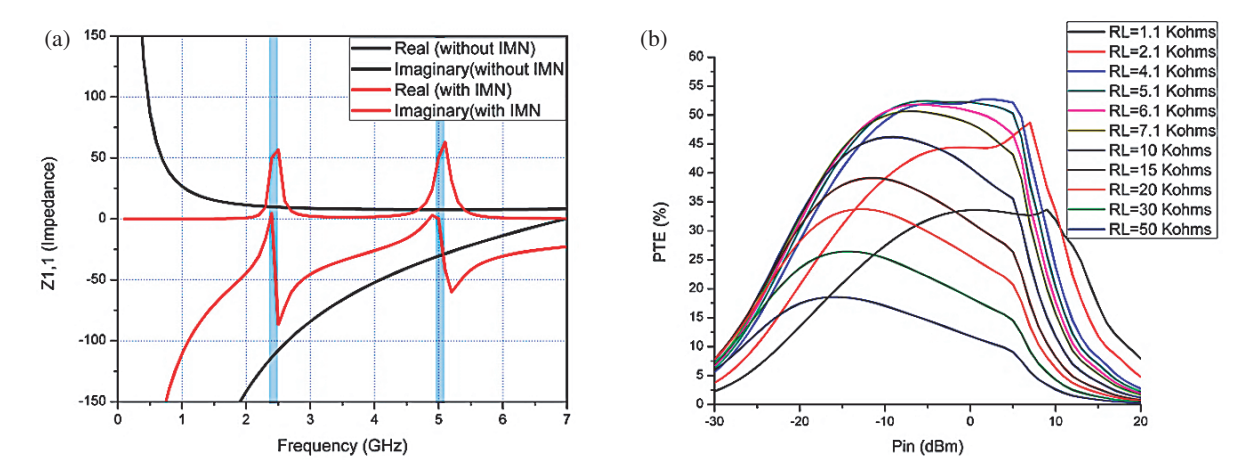


**FIGURE 16.** (a) Impedance  $(Z_1, 1)$  plot of the rectifier with and without IMC. (b) PTE vs Pin with different  $R_L$ .

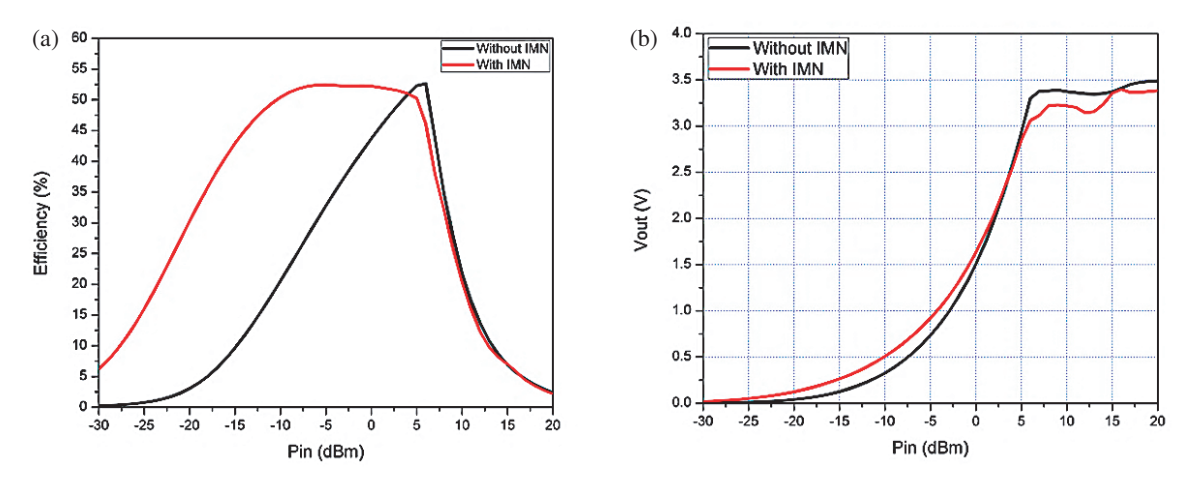


FIGURE 17. Comparison of rectifier with and without IMC (a) PTE vs Power input, (b) Vout vs Power input.

 $P_{input\ AC}$  is the rectifier input RF incident power; and  $R_L$  is the resistance load.

To obtain maximum PTE, all the harvested RF AC power by the dual-band receiver must be transferred to the rectifier input with minimum loss, and it is done by proposed modified Pi-section IMC. The rectifier impedance in the presence and absence of the IMC is shown in Figure 16(a). The main function of the IMC is to approximate the impedance of the receiver with the impedance of the rectifier. For this purpose, the impedances of the rectifier at both operating frequencies are obtained in the absence of IMC, and they are  $9.8 - j113.57 \Omega$ and  $7.6 - j30.46 \Omega$  at 2.4 GHz and 5 GHz respectively obtained from the impedance plot. These impedances of the rectifier are matched to the  $50 \Omega$  receiver impedance by using modified Pisection IMC. After matching, the impedances of the rectifier are  $50 + j0.6 \Omega$  and  $50 + j0.16 \Omega$  observed at 2.4 GHz and 5 GHz, respectively. To analyze the working of the projected rectenna at a broad range of resistance load, the PTE at 2.4 and 5 GHz frequencies with different resistance values over the range 1.1– 50 K $\Omega$  is evaluated concerning  $P_{in}$  variations and shown in Figure 16(b). It is observed that the PTE is less sensitive over the range of  $4.1-7.1 \text{ K}\Omega$  load, and outside this range of resistance values, the PTE decreases. A optimum load resistance of  $5.1~\mathrm{K}\Omega$  is considered which has maximum PTE over a broad range of low input power. To study the behavior of the rectifier at both operating frequencies, the PTE of the rectifier and output DC voltage are obtained by tuning the input-power level over a wide range from  $-30~\mathrm{dBm}$  to  $20~\mathrm{dBm}$  with an optimum load resistance of  $5.1~\mathrm{K}\Omega$  in the presence and absence of the IMC, shown in Figure 17.

From Figure 17(a), the efficiency of the rectifier without IMC is above 50% from 4 dBm to 6 dBm with a maximum of 52.64% at 6 dBm, and in the presence of IMC, it is above 50% from  $-10 \,\mathrm{dBm}$  to  $5 \,\mathrm{dBm}$  with maximum 52.45% at  $-5 \,\mathrm{dBm}$ input power. The rectifier efficiency is above 40% for a wide range of low-input power, i.e., from  $-16 \, dBm$  to  $7 \, dBm$ . From Figure 17(b), the rectifier output voltage is large in the presence of IMC,  $V_{out}=51\,\mathrm{mV},\,124\,\mathrm{mV},\,236\,\mathrm{mV},\,507\,\mathrm{mV},$  and  $1.0\,\mathrm{V}$  compared with the absence of IMC,  $V_{out} = 11\,\mathrm{mV}$ , 40 mV, 126 mV, 327 mV, and 734 mV at low input power levels  $P_{in} = -25 \,\mathrm{dBm}, -20 \,\mathrm{dBm}, -15 \,\mathrm{dBm}, -10 \,\mathrm{dBm},$  and -5 dBm, respectively, and reaches approximately same values as the input power rises.  $V_{out}$  and efficiency are 1.63 V and 52.22% in the presence of IMC and 1.5 V and 43.65% in the absence of IMC at 0 dBm input power level. The increase in the efficiency at low input power levels and then fall at higher input



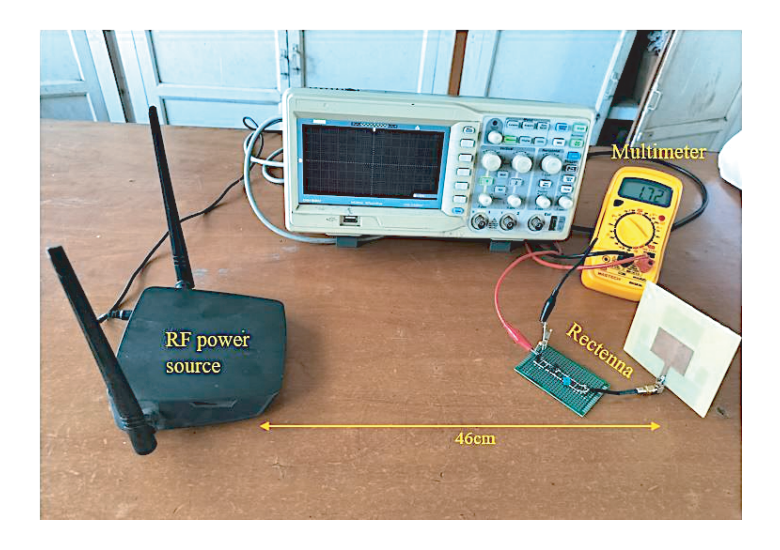


FIGURE 18. Fabricated rectenna calibration setup.

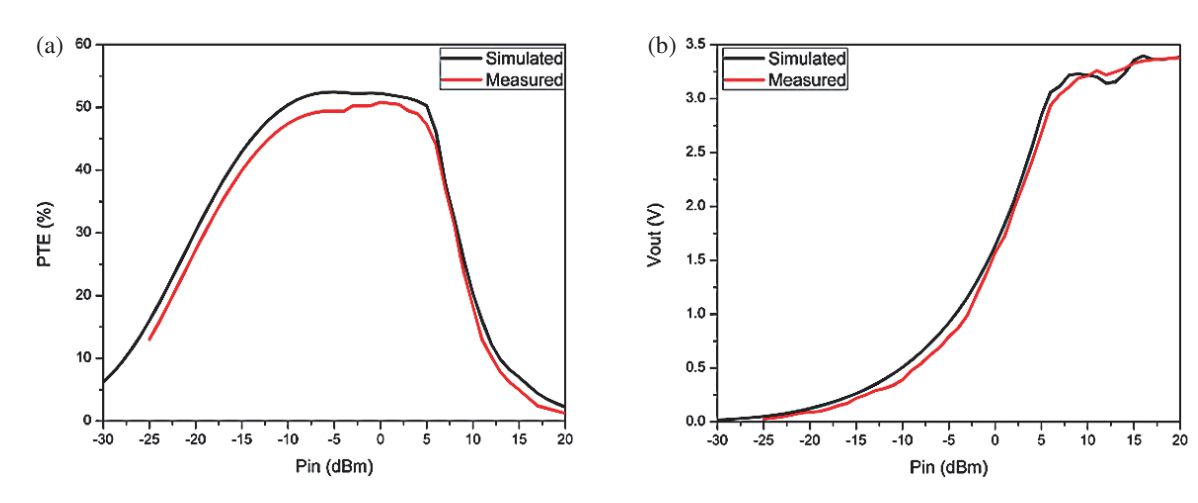


FIGURE 19. Correlation of calibrated and simulated results. (a) PTE vs Pin. (b) Vout vs Pin.

levels is are due to the internal parameters of the diode HSMS-2852 which makes it more apt for low power range. In both the rectifiers matched and not-matched, the efficiencies rise as a rise in the input power level up to reverse breakdown voltage of the diode is reached after rectifier efficiency degrades at higher input power levels, and also saturation effect occurs at specific higher input level then the rectifying capability of the diode lost which result in efficiency fall.

# 4. CALIBRATION OF THE RECTENNA

The prototype RF receiving antenna and rectifier are fabricated separately and integrated into the rectenna by connecting them with a  $50\,\Omega$  male-to-female SMA connector during the assembly process. The measurement setup to evaluate the behavior of the manufactured prototype rectenna is carried out as per [34] in the indoor ambiance, and it is shown in Figure 18.

The calibration setup consists of an RF source specifically a NETGEAR (AC1200) WLAN router module, which simultaneously generates dual-band frequencies of 2.4 GHz and

5 GHz. The fabricated rectenna is connected to a multimeter (voltmeter) to measure and calibrate the output DC voltage. The rectenna is located in front of the RF source which has built-in aspect to change RF signal power which makes measurement easy. By varying RF source power, the output voltage is measured at each instant. The separation between the transmitting RFAC generator and the rectenna is considered as 46 cm to attain the maximum PTE. Using the Friis transmission equation, the power received by the rectenna is obtained, and it is given by the equation as follows.

$$P_R = G_T P_T G_R \left(\frac{\lambda}{4\pi r}\right)^2 \tag{7}$$

where  $G_T$  and  $G_R$  are the gains of the transmitter and receiver;  $\lambda$  is the operating wavelength;  $P_T$  is the power transmitted by the RF source; and r is the gap between the receiving antenna and the RF source.

The calibrated and simulated PTE and output DC voltage comparison plot are shown in Figure 19. From Figure 19, it



FIGURE 20. (a) The measurement setup for driving LED indicator and wall clock. (b) Back view of the wall clock.

**TABLE 3**. Correlation of the prototype rectenna with earlier studies for RF energy harvesting.

References	Antenna Size (mm <sup>3</sup> )	Rectifier Topology	Frequency (GHz)	Diode	Pin (dBm)	PTE (%)	Vout (V)
[12]	$35 \times 37 \times 1.6$	Delton voltage quadruple	2.45, 3.5	HSMS 2852	0	60, 53	1.22, 1.13
[18]	$95 \times 65 \times 5$	Single series diode	3.5, 5.8	SMS 7630	0	44, 29	656.88 m
[19]	$80 \times 80 \times 5.07$	Voltage doubler	2.45, 5	HSMS 286B	0	68.83, 49.9	0.167, 0.236
[21]	$50 \times 50 \times 0.76$	Single series diode	0.7, 1.4	SMS 7630	-6.5	74	0.7
[27]	$60 \times 50 \times 6$	Single series diode	3.5, 5.8	HSMS 2860	5	56, 43	1.31, 1.16
[31]	$67.5 \times 71.5 \times 1.016$	Voltage doubler	2.45, 5.8	HSMS 2852	10.5	65.1, 38.4	2.96, 2.41
This work	$60 \times 50 \times 1.6$	Voltage doubler	2.4, 5	HSMS 2852	0	50	1.57

is realized that the calibrated rectenna PTE is above 45% from -12 dBm to 5 dBm input power level with a maximum of 50% at 0 dBm. The measured PTE is less than simulated one because of the inappropriate soldering of the SMD elements in the rectifier circuit and also the nonlinear nature at higher frequencies of the rectifier elements. The maximum DC voltage and power of 3.4 V and 2.26 mW are noticed at 20 dBm and 1.57 V with 483 µW at 0 dBm input level when the rectifier engages simultaneously at frequencies 2.4 GHz and 5 GHz with 5.1 K $\Omega$  load. The prototype rectenna can power up different household low-power sensors like a small calculator-2 μW, digital thermometer-20 μW, smoke detector-55 μW, and wall clock-120 µW, and personal low-power sensors like a wristwatch-10 μW, wearable-60 μW, mouse-10 μW, and Wi-Fi flash memory-210 µW [35]. By comparing the measured and simulated results it is realized that they are nearly correlated to each other. The available rectenna designs by the previous researchers are compared with the proposed rectenna model to validate its performance, and the comparisons are summarized in Table 3.

The rectenna output is used to drive the LED indicator and wall clock as mentioned above, and the measurement setup is shown in Figure 20. The receiving antenna is placed at a distance of 40 cm from the RF power source. At this distance, the output of the rectenna is 1.57 V, and it is dropped to 1.19 V due to low input impedance of the boost converter. The output of the rectenna is connected to the input of the DC-DC boost converter which generates a stable 5 V output and is able to drive LED indicator and wall clock simultaneously.

# 5. CONCLUSION

In this study, an efficient dual-band rectenna with a wide input power range for electromagnetic EH at Wi-Fi frequencies 2.4 GHz and 5 GHz and a step-up DC-DC boost converter is reported. A simple rectangular patch antenna with a PG plane loaded with parasitic stubs helps in prevailing resonance at 2.4 GHz and 5 GHz frequencies with a gain of 2.45 dBi and 4.84 dBi, respectively. The impedance of the recommended antenna is attained at  $50 \Omega$  for both the operating frequencies by tuning parameters of the ground plane with parasitic stubs1 and stub2. A compact single-stage Greinacher voltage doubler rectifier with dual-band modified Pi-section IMC is designed with HSMS-2852 Schottky diode to operate in the wide low input power levels from  $-25 \, \mathrm{dBm}$  to  $10 \, \mathrm{dBm}$ . The modified Pi-section IMC is formed by cascading two L-section IMCs to match the rectifier impedances of  $9.8 - j113.57 \Omega$  and  $7.6 - j30.46 \Omega$  with the antenna  $50 \Omega$  impedance to maximize RF AC-DC PTE at low-input power levels. The projected rectifier gained above 40% measured PTE for  $-12 \, \mathrm{dBm}$  to  $5 \, \mathrm{dBm}$ with 50% at 0 dBm input power level when 2.4 GHz and 5 GHz are applied simultaneously. The measured output voltage is 1.57 V at 0 dBm with a load resistance of 5.1 K $\Omega$ . The output of the rectenna is connected to step-up DC-DC boost converter which is used to power an LED indicator and a wall clock. Future work includes the design of a wearable multiband rectenna with compact size for WBAN applications and improving the efficiency of the rectenna.



# **ACKNOWLEDGEMENT**

The authors wish to express their profound gratitude to Universiti Teknikal Malaysia Melaka (UTeM) for their generous support. This work was made possible through the grant PJP/2024/FTKEK/PERINTIS/S01388. Their assistance and resources have been instrumental in the successful completion of this research.

# **REFERENCES**

- [1] Halimi, M. A., T. Khan, Nasimuddin, A. A. Kishk, and Y. M. M. Antar, "Rectifier circuits for RF energy harvesting and wireless power transfer applications: A comprehensive review based on operating conditions," *IEEE Microwave Magazine*, Vol. 24, No. 1, 46–61, 2023.
- [2] Mansour, M. M., S. Torigoe, S. Yamamoto, and H. Kanaya, "Compact and simple high-efficient dual-band RF-DC rectifier for wireless electromagnetic energy harvesting," *Electronics*, Vol. 10, No. 15, 1764, 2021.
- [3] Amer, A. A. G., S. Z. Sapuan, N. B. Othman, A. A. Salem, A. J. A. Al-Gburi, and Z. Zakaria, "A wide-angle, polarizationinsensitive, wideband metamaterial absorber with lumped resistor loading for ISM band applications," *IEEE Access*, Vol. 12, 42 629–42 641, 2023.
- [4] Amer, A. A. G., N. Othman, S. Z. Sapuan, A. Alphones, M. F. Hassan, A. J. A. Al-Gburi, and Z. Zakaria, "Dual-band, wideangle, and high-capture efficiency metasurface for electromagnetic energy harvesting," *Nanomaterials*, Vol. 13, No. 13, 2015, Jul. 2023.
- [5] Mansour, M. M. and H. Kanaya, "Efficiency-enhancement of 2.45-GHz energy harvesting circuit using integrated CPW-MS structure at low RF input power," *IEICE Transactions on Electronics*, Vol. 102, No. 5, 399–407, 2019.
- [6] Shafique, K., B. A. Khawaja, M. D. Khurram, S. M. Sibtain, Y. Siddiqui, M. Mustaqim, H. T. Chattha, and X. Yang, "Energy harvesting using a low-cost rectenna for Internet of Things (IoT) applications," *IEEE Access*, Vol. 6, 30 932–30 941, 2018.
- [7] Pandey, R., A. K. Shankhwar, and A. Singh, "Design and analysis of rectenna at 2.42 GHz for Wi-Fi energy harvesting," *Progress In Electromagnetics Research C*, Vol. 117, 89–98, 2021.
- [8] Uzun, Y., "Design of an efficient triple band RF energy harvester," Applied Computational Electromagnetics Society Journal, Vol. 30, No. 12, 1286–1293, 2015.
- [9] Wang, C., J. Zhang, S. Bai, D. Chang, and L. Duan, "A multi-band compact flexible energy collector for wearable or portable IoT devices," *IEEE Antennas and Wireless Propagation Letters*, Vol. 22, No. 5, 1164–1168, 2023.
- [10] Bougas, I. D., M. S. Papadopoulou, A. D. Boursianis, S. Nikolaidis, and S. K. Goudos, "Dual-band rectifier circuit design for IoT communication in 5G systems," *Technologies*, Vol. 11, No. 2, 34, 2023.
- [11] Papadopoulou, M. S., A. D. Boursianis, C. K. Volos, I. N. Stouboulos, S. Nikolaidis, and S. K. Goudos, "High-efficiency triple-band RF-to-DC rectifier primary design for RF energy-harvesting systems," *Telecom*, Vol. 2, No. 3, 271–284, 2021.
- [12] Wang, M., Y. Fan, L. Yang, Y. Li, J. Feng, and Y. Shi, "Compact dual-band rectenna for RF energy harvest based on a tree-like antenna," *IET Microwaves, Antennas & Propagation*, Vol. 13, No. 9, 1350–1357, 2019.
- [13] Zapata Ochoa, E. A., F. L. Giraldo, and G. D. Góez, "Dual band rectenna for wireless energy harvesting in the 2.40 GHz and

- 5.38 GHz," TecnoLógicas, Vol. 25, No. 55, e2384, 2022.
- [14] Mohd Noor, F. S., Z. Zakaria, H. Lago, and M. A. M. Said, "Dual-band aperture-coupled rectenna for radio frequency energy harvesting," *International Journal of RF and Microwave Computer-Aided Engineering*, Vol. 29, No. 1, e21651, 2019.
- [15] Dardeer, O. M. A., H. A. Elsadek, and E. A. Abdallah, "Compact broadband rectenna for harvesting RF energy in WLAN and WiMAX applications," in 2019 International Conference on Innovative Trends in Computer Engineering (ITCE), 292–296, Aswan, Egypt, 2019.
- [16] Abdullah Al-Gburi, A. J., I. M. Ibrahim, and Z. Zakaria, "Gain enhancement for whole ultra-wideband frequencies of a microstrip patch antenna," *Journal of Computational and Theoretical Nanoscience*, Vol. 17, No. 2-3, 1469–1473, 2020.
- [17] Rajawat, A. and P. K. Singhal, "Design and analysis of inset fed wide-band rectenna with defected ground structure," *Journal* of Circuits, Systems and Computers, Vol. 29, No. 03, 2050047, 2020.
- [18] Derbal, M. C. and M. Nedil, "A high gain dual band rectenna for RF energy harvesting applications," *Progress In Electromagnetics Research Letters*, Vol. 90, 29–36, 2020.
- [19] Mohd Noor, F. S., Z. Zakaria, H. Lago, and M. A. M. Said, "Dual-band aperture-coupled rectenna for radio frequency energy harvesting," *International Journal of RF and Microwave Computer-Aided Engineering*, Vol. 29, No. 1, e21651, 2019.
- [20] Saravanan, M. and A. Priya, "Design of tri-band microstrip patch rectenna for radio frequency energy harvesting system," *IETE Journal of Research*, Vol. 68, No. 4, 2410–2415, 2022.
- [21] Aboualalaa, M., I. Mansour, A. B. Abdelrahman, A. Allam, M. Abo-zahhad, H. Elsadek, and R. K. Pokharel, "Dual-band CPW rectenna for low input power energy harvesting applications," *IET Circuits, Devices & Systems*, Vol. 14, No. 6, 892– 897, 2020.
- [22] Benkalfate, C., A. Ouslimani, A.-E. Kasbari, and M. Feham, "A new compact triple-band triangular patch antenna for RF energy harvesting applications in IoT devices," *Sensors*, Vol. 22, No. 20, 8009, 2022.
- [23] Halimi, M. A., T. Khan, S. K. Koul, and S. R. Rengarajan, "A dual-band rectifier using half-wave transmission line matching for 5G and Wi-Fi bands RFEH/MPT applications," *IEEE Microwave and Wireless Technology Letters*, Vol. 33, No. 1, 74–77, 2023.
- [24] Muhammad, S., J. J. Tiang, S. K. Wong, A. Smida, R. Ghayoula, and A. Iqbal, "A dual-band ambient energy harvesting rectenna design for wireless power communications," *IEEE Access*, Vol. 9, 99 944–99 953, 2021.
- [25] Halimi, M. A., D. Surender, T. Khan, A. A. Kishk, and S. R. Rengarajan, "A multistepped transmission line matching strategy based triple-band rectifier for RFEH/WPT applications," *IEEE Microwave and Wireless Components Letters*, Vol. 32, No. 8, 1007–1010, 2022.
- [26] Hameed, Z. and K. Moez, "Design of impedance matching circuits for RF energy harvesting systems," *Microelectronics Journal*, Vol. 62, 49–56, 2017.
- [27] Surender, D., M. A. Halimi, T. Khan, F. A. Talukdar, and Y. M. M. Antar, "Circularly polarized DR-rectenna for 5G and Wi-Fi bands RF energy harvesting in smart city applications," *IETE Technical Review*, Vol. 39, No. 4, 880–893, 2022.
- [28] Polaiah, G., K. Krishnamoorthy, and M. Kulkarni, "A compact dual-band rectenna for RF energy harvesting," in 2019 IEEE Indian Conference on Antennas and Propagation (InCAP), 1–4, Ahmedabad, India, 2019.



- [29] Khemar, A., A. Kacha, H. Takhedmit, and G. Abib, "Design and experiments of a dual-band rectenna for ambient RF energy harvesting in urban environments," *IET Microwaves, Antennas & Propagation*, Vol. 12, No. 1, 49–55, 2018.
- [30] Aboualalaa, M. and H. Elsadek, "Rectenna systems for RF energy harvesting and wireless power transfer," in *Recent Wireless Power Transfer Technologies*, 1–24, P. Pinho (ed.), IntechOpen, 2020.
- [31] Li, L., R. Xu, J. Cao, X. Li, and J. Nan, "A compact loop-shaped dual-band omnidirectional rectenna for RF energy harvesting," *Progress In Electromagnetics Research M*, Vol. 125, 1–9, 2024.
- [32] Balanis, C. A., Antenna Theory: Analysis and Design, John Wiley & Sons, 2016.
- [33] Pozar, D. M., Microwave Engineering, John Wiley & Sons, 2011.
- [34] Awais, Q., Y. Jin, H. T. Chattha, M. Jamil, H. Qiang, and B. A. Khawaja, "A compact rectenna system with high conversion efficiency for wireless energy harvesting," *IEEE Access*, Vol. 6, 35 857–35 866, 2018.
- [35] Georgiou, O., K. Mimis, D. Halls, W. H. Thompson, and D. Gibbins, "How many Wi-Fi APs does it take to light a lightbulb?" *IEEE Access*, Vol. 4, 3732–3746, 2016.